

Overview of Additively Manufactured TPS Proposed Flight Test and Earth Re-entry Capsule Design

David J. Blette
 NASA Langley Research Center
 1 N Dryden St
 Hampton, VA 23681
 david.j.blette@nasa.gov

Adam T. Sidor
 NASA Johnson Space Center
 2101 E NASA Pkwy
 Houston, TX 77058
 adam.t.sidor@nasa.gov

John E. Theisinger
 NASA Langley Research Center
 1 N Dryden St
 Hampton, VA 23681
 john.e.theisinger@nasa.gov

Ali D. Omidy
 NASA Johnson Space Center
 2101 E NASA Pkwy
 Houston, TX 77058
 ali.d.omidy@nasa.gov

Abstract—A flight mechanics overview is presented of an Earth flight test designed to investigate a novel, 3D printed thermal protection system (TPS) that is currently in development at NASA as part of the Additive Manufacturing of Thermal Protection Systems project. The project is pioneering a method to print a thermal protection system onto an entry vehicle forebody one layer at a time. This method reduces labor and complexity as compared to traditional manufacturing methods while increasing mission-dependent customization of through-depth materials properties. The flight test has three objectives. First, subject the forebody stagnation point of a capsule equipped with additively manufactured TPS (AMTPS) material to peak heat fluxes in excess of $100 W/cm^2$. Second, capture in-flight data to enable flight reconstruction and AMTPS material thermal response model improvement. Third, recover the capsule with data storage and forebody AMTPS intact to enable post-flight inspection and analysis of AMTPS performance.

The flight test trajectory is designed to achieve a peak stagnation point, cold-wall, entry heat flux of $135 W/cm^2$. Flight mechanics simulations are performed using the Program to Optimize Simulated Trajectories II (POST2) and Monte-Carlo analysis yields statistical percentiles on vehicle performance at key points along the trajectory. Based on the flight mechanics analysis presented in this paper, a prototype capsule was designed, partially fabricated, and underwent preliminary component stress testing in preparation for fabrication of the flight unit capsule. The capsule outer mold line is a modified version of the heritage Mars Microprobe geometry. The capsule has a 0.356 m diameter, a 30 kg mass, and a hypersonic ballistic coefficient of $300 kg/m^2$. Sensor selection is guided by flight dynamics simulations with the goal of resolving the re-entry heating pulse. On-board instrumentation include forebody and aftbody pressure sensors and thermocouples, a 9-axis IMU, a GPS receiver, and an Iridium satellite modem, all of which collect and store data throughout flight via on-board avionics systems. A two-stage parachute system is designed to decelerate the capsule to touchdown velocities that will not result in significant fracture or deformation of the charred AMTPS material at ground impact.

TABLE OF CONTENTS

1. INTRODUCTION.....	1
2. AMTPS MATERIAL OVERVIEW	2
3. FLIGHT TEST MISSION OVERVIEW.....	3
4. FLIGHT MECHANICS ANALYSIS AND CAPSULE DESIGN	3
5. AEROTHERMODYNAMIC ANALYSIS	8

6. PROTOTYPE CAPSULE FABRICATION STATUS	9
7. FURTHER WORK	10
8. SUMMARY	10
ACKNOWLEDGMENTS	10
REFERENCES	10
BIOGRAPHY	11

1. INTRODUCTION

Additive Manufacturing of Thermal Protection Systems (AMTPS) is a multi-center NASA Early Career Initiative (ECI) project that started in Fiscal Year (FY) 2021 and has continued through the 1st half of FY 2023. The AMTPS project originated at NASA’s Johnson Space Center in 2017 to explore the feasibility and applicability of additive manufacturing (AM) for spacecraft heat shields [1]. The automated approach of AM can improve upon traditionally manual, labor-intensive manufacturing and integration processes for TPS. Potential benefits include reduced cost, shorter lead times, and improved consistency. Furthermore, depositing the TPS directly onto an underlying structure during processing simplifies integration. Three primary goals were outlined for the project:

1. Develop and characterize a printable, graded TPS architecture;
2. Build and test a Manufacturing Demonstration Unit (MDU) up to 1.0 meter in diameter that demonstrates the newly developed material formation and direct integration process;
3. Design and build a flight test capsule equipped with an AMTPS heat shield for a follow-on hypersonic flight test to demonstrate end-to-end manufacturing and flight performance of the material.

This paper provides an overview of the flight test mission and capsule designed to meet the objectives of the final goal: designing, building, and flying a small capsule with an AMTPS heat shield in relevant entry conditions.

Section 2 presents an overview of the material formulation and deposition process used to develop 3D-printed heat shields. The motivation for performing an Earth flight test and a detailed mission concept of operations is discussed in Section 3. Section 4 talks about the flight mechanics simulation developed to analyze the flight test performance and generate data necessary to guide re-entry capsule design

decisions. Section 5 presents an aerothermal analysis of the capsule flow field at the peak heat flux condition of the nominal flight trajectory. Section 6 discusses the status of the prototype capsule manufacturing and integration activities. The work remaining to be completed as part of this body of work is enumerated in Section 7. Finally, Section 8 summarizes the contents of this publication.

2. AMTPS MATERIAL OVERVIEW

The project leverages a method of additive manufacturing called direct ink writing (DIW). DIW uses rheologically tailored "inks" that are extruded through a nozzle and deposited onto a build surface, such as a capsule forebody structure. The project's iteration of DIW uses high temperature thermoset resins loaded with fiber fillers to impart strength and microsphere fillers to reduce density. Importantly, a rheology modifier is added to the resin to yield a shear thinning paste, i.e., a material that decreases in viscosity with applied pressure. This property, critical to the DIW process, allows the uncured TPS material to be pumped through a delivery system yet hold its shape once deposited onto the vehicle structure. The DIW process is illustrated in Figure 1. In this way, the TPS is built up layer-by-layer. Once the full thickness is deposited, the TPS is thermally cured, becoming rigid and bonding to the vehicle structure at the same time. The outer mold line is then machined to the desired thickness and surface finish.

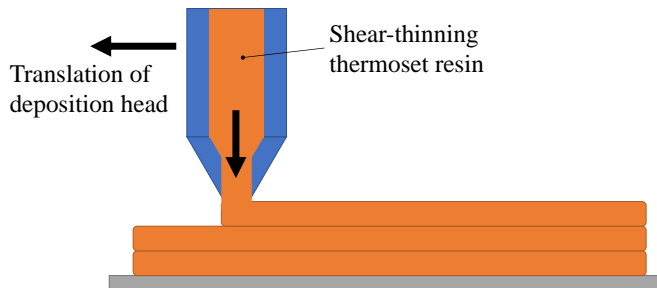


Figure 1: Conceptual diagram of a direct ink write (DIW) process [1].

The layer-by-layer approach enables material formulation to be varied through the thickness. The AMTPS project developed a dual layer system consisting of a higher density, robust layer on the outer surface with a lower density, lower thermal conductivity insulating layer underneath. Both formulations are based on the same commercially available phenolic resin but loaded with different packages of solid fillers. The robust layer contains glass microspheres and carbon fibers, while the insulating layer contains glass microspheres and glass fibers. Flexibility in layer formulation and thickness allows the heat shield to be tailored to meet the unique aerothermal requirements of a given mission. Additional information on AMTPS material and process development can be found in Reference [1].

The project has extensively characterized its specific phenolic material composition in ground testing, including quantification of both mechanical and thermal properties. These properties form the basis of a material database that will be used for modeling the thermomechanical performance of the TPS

during flight. Ground testing also included two test series in the NASA Ames Research Center Aerodynamic Heating Facility (AHF). The first test series, completed in November 2021, consisted of 15 AMTPS 4-inch iso-q specimens; these specimens have a shape ensuring constant heat flux over the entire windward surface. Exposures were 30 seconds with stagnation point heat flux of 132 W/cm^2 and pressure of 3.7 kPa. Images of two pre- and post-exposure test articles are shown in Figure 2. The second arcjet series, completed in November 2022, again tested 4-inch iso-q models but at a higher heating condition of 232 W/cm^2 with stagnation pressure of 8.4 kPa. In both series, the AMTPS articles performed well with little or no recession. Backface temperatures, measured via thermocouples, were well below those typically applied for a bondline temperature.

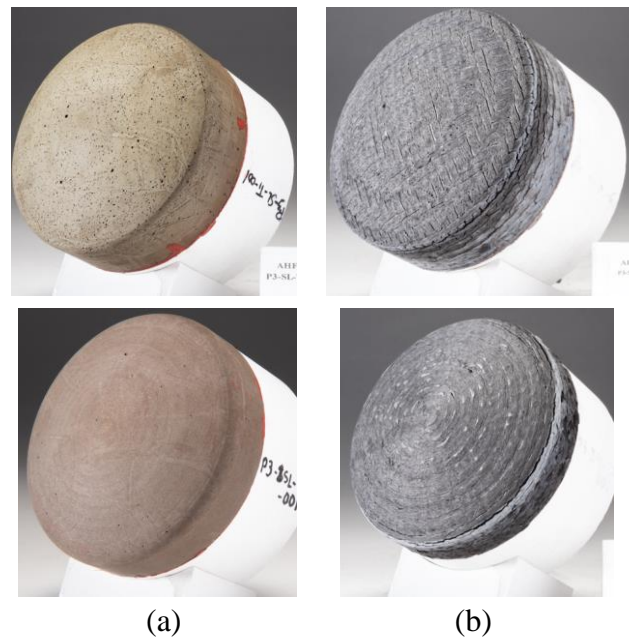


Figure 2: AMTPS arcjet models (a) pre- and (b) post-exposure.

Both a forebody and backshell TPS will be manufactured for the flight capsule. The forebody heat shield uses the two layer AMTPS system (robust on top of insulating layer) while the backshell will only use the insulating layer to reduce weight. An adhesive, currently under development, will serve as an intermediate layer between the TPS and the structure to facilitate bonding. The TPS and adhesive are co-cured in a single cycle. Both the forebody and backshell TPS will be printed using the DIW process described above in a manufacturing cell being developed under a partnership with Oak Ridge National Laboratory. The AMTPS manufacturing cell, shown in Figure 3, consists of a robot arm, a rotating/tilting table, and a pumping system. The system can print parts up to 1.0 m by 1.0 m by approximately 2.0 m tall. The figure shows a test print of a forebody TPS for a small capsule similar in size to the flight test capsule discussed in the present paper.

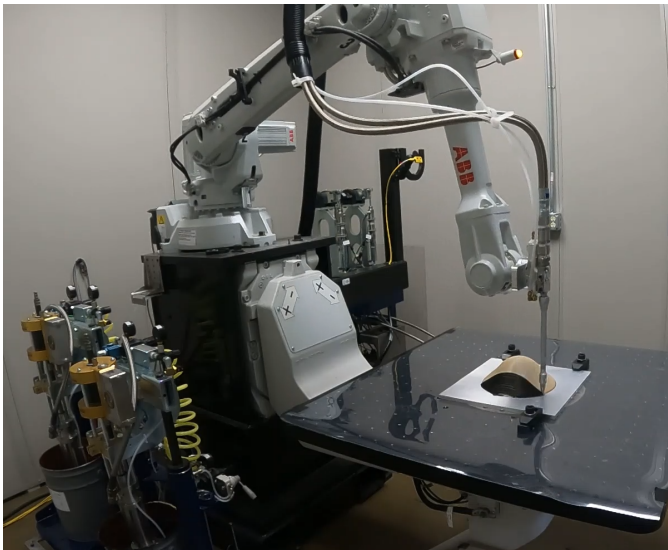


Figure 3: AMTPS robotic cell under development at Oak Ridge National Laboratory.

3. FLIGHT TEST MISSION OVERVIEW

Motivation for High Energy Sounding Rocket Flight Test

AMTPS material is currently undergoing a variety of ground-based testing as part of the material and process formulation component of the larger technology development campaign. Small 4 inch coupons are subjected to heat fluxes in excess of 100 W/cm^2 for durations exceeding 20 seconds in an arcjet testing facility. These small-coupon tests are geared toward material formulation development and determining individual and layered material properties. A full scale arcjet test is currently being planned for a 14 inch diameter heat shield integrated onto a metal capsule support structure and will be completed prior to the sounding rocket test described in this paper. The proposed sounding rocket test will increase the technology readiness level (TRL) of the AMTPS material through demonstration of an end-to-end test of the AMTPS manufacturing process, integration onto a capsule substructure, instrumentation infusion into the AMTPS material, flight, and capsule recovery. The flight test will subject the instrumented AMTPS heat shield to inertial and aerodynamic stresses during a representative heating environment that is relevant to a variety of commercial and government missions that may benefit from the AMTPS advantages over traditional TPS materials and manufacturing processes. The successful completion of this flight will yield lessons-learned and serve as validation of the AMTPS material formulation and manufacturing process.

Mission Concept of Operations

The flight test objectives are to subject the forebody stagnation point of a capsule equipped with AMTPS material to peak heat fluxes in excess of 100 W/cm^2 , capture in-flight data to enable flight reconstruction and AMTPS material thermal response model improvement, and recover the capsule with data storage and forebody AMTPS intact to enable post-flight inspection and analysis of AMTPS performance. To meet these objectives, a launch provider was contracted to design a launch vehicle trajectory that could deliver the test capsule to an apogee yielding the desired peak heat fluxes upon re-entry. A capsule outer mold line (OML) following that of the Mars Microprobe [2] vehicle was chosen due to

the extensive heritage body of work demonstrating favorable stability and aerodynamic properties[2], [3], [4].

The flight test concept of operations is presented in Figure 4. The reference flight test will launch from White Sands Missile Range in New Mexico. The launch vehicle is stabilized using a canard system and, accordingly, does not accumulate appreciable roll rates during ascent. Therefore, the capsule must be capable of self-righting upon entering the atmosphere as it will not be roll-stabilized at any specific orientation prior to entry. Sixty seconds after launch, at an altitude of 126 km, the capsule separates from the rocket payload section and ascends to a peak altitude of 434 km at 325 s after launch. The capsule is a ballistic entry vehicle capable of self-righting itself from any orientation once appreciable atmosphere is encountered around 110 km altitude. Figure 5 shows altitude versus Mach number for the entry segment of the simulated nominal flight trajectory. An in-depth discussion of the simulation assumptions and inputs is presented in Section 4. In the present context, Figure 5 supplements the illustrated concept of operations in Figure 4 with the coupled relationship between vehicle altitude and speed during re-entry. A peak re-entry Mach number of 9.1 occurs 600 s after launch at 93 km altitude. Peak stagnation point heat flux of 135 W/cm^2 (cold-wall) occurs 30 s later at 28 km altitude. The capsule logs data from on-board instrumentation starting at capsule egress from the launch vehicle and continuing until capsule touchdown. On-board instrumentation includes forebody and aftbody pressure sensors and thermocouples, a 9-axis IMU, and a GPS receiver. At 2.55 km altitude and 710 s after launch, the drogue parachute deploys at a dynamic pressure of 4.3 kPa. The main parachute is extracted by the drogue parachute 25 s later at 1.4 km altitude and 0.6 kPa of dynamic pressure. While descending under parachutes, the capsule transmits GPS tracking data to the Iridium Satellite network to aid recovery operations. The capsule touches down in the desert at 7.9 m/s, approximately 950 s after launching. 540 seconds elapse between capsule deployment from the launch vehicle payload section and atmospheric re-entry; 350 seconds elapse from atmospheric re-entry to capsule touchdown.

This flight test concept provides an opportunity for a secondary TPS test. The ascent vehicle nose cone jettisons prior to capsule egress and is recoverable after descending under a parachute to the ground. The exterior skin of the nose cone can be equipped with patches of instrumented TPS coupons that will experience ascent heating, log data, and can be recovered for inspection and data analysis. The present paper focuses on the primary capsule payload of the mission and neglects further discussion of the ascent vehicle nose cone.

4. FLIGHT MECHANICS ANALYSIS AND CAPSULE DESIGN

Flight Simulation Model Composition

The Program to Optimize Simulated Trajectories II (POST2) [5] is used to perform flight mechanics analysis on the capsule trajectory and aid in capsule design. The mission simulation incorporates the following models:

1. Ellipsoidal planet model utilizing data from the NASA Earth Fact Sheet [6]
2. 8th-order spherical harmonics gravity model utilizing data from GRACE satellite GGM03C
3. Surface terrain defined by digital elevation maps from USGS

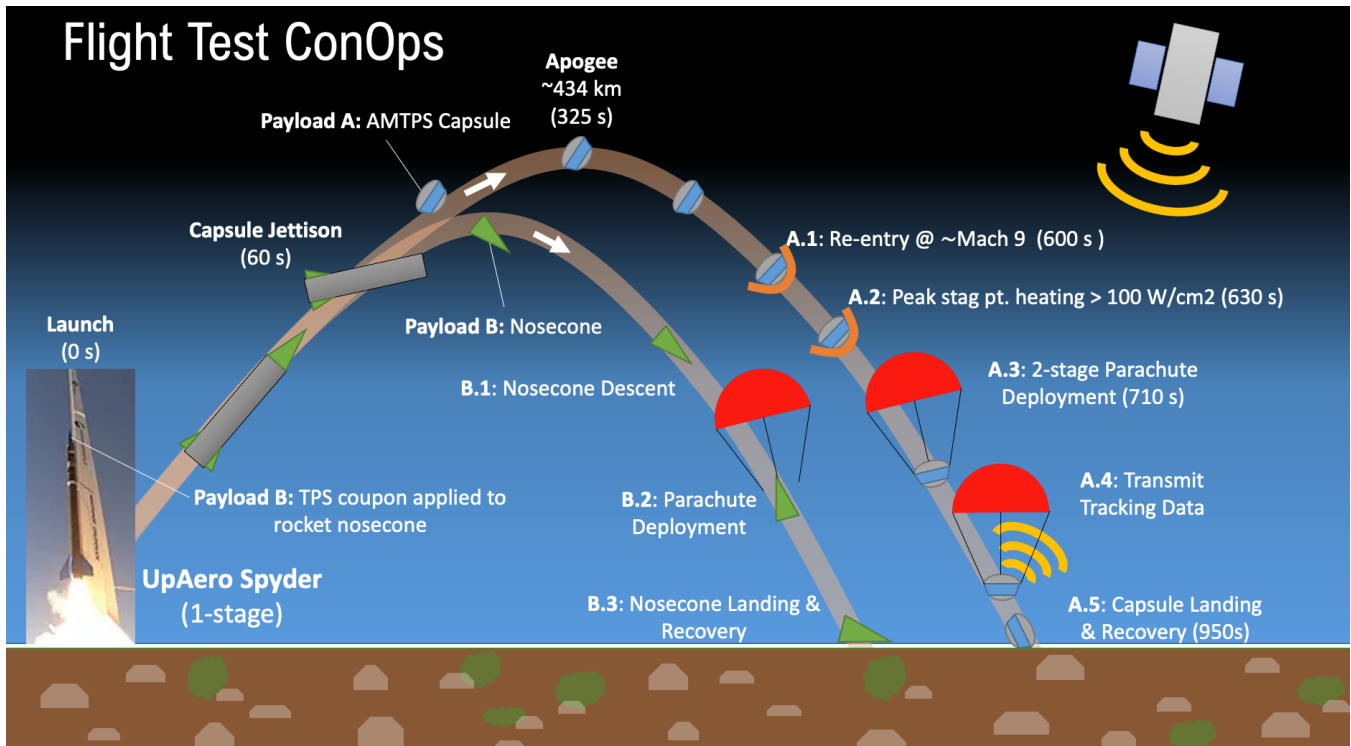


Figure 4: AMTPS flight test concept of operations.

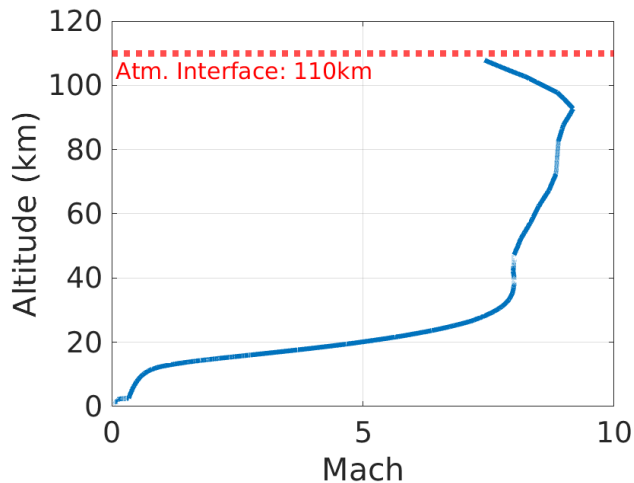


Figure 5: Altitude above geoid versus Mach number for the entry segment of the nominal trajectory.

4. EarthGRAM 2010 atmosphere model [7]
5. Aerodynamics model using Mars Microprobe data adapted for Earth and capsule geometry modifications
6. Sutton-Graves aerothermodynamic model
7. Stagnation point pressure model using chemical equilibrium analysis [8]
8. Parachute drag model based on fixed inflation distance assumptions [9]

An 8001 case, six degree-of-freedom Monte Carlo analysis is performed using capsule dynamic state distributions at launch vehicle egress, randomized atmospheric perturbations,

capsule mass and inertia perturbations, aerodynamic coefficient uncertainty distributions, and variations in parachute inflation parameters. Capsule state vector inputs to the POST2 simulation were provided by the contracted launch provider in the form of dispersions in position, velocity, and attitude rates at the point of capsule egress from the launch vehicle payload section. The atmosphere model draws from 2010 Earth Global Reference Atmosphere Model (GRAM) 3σ data for atmospheric density, pressure, and winds based on longitude, latitude, and altitude points along the vehicle trajectory. Capsule mass properties are dispersed using heritage dispersions for similar capsules from the literature [10], [11] and re-enforced by CAD studies perturbing individual capsule component masses and locations. Aerodynamic coefficient uncertainties are leveraged from heritage uncertainties for the Mars Microprobe and updated for specific capsule geometry modifications and an Earth atmosphere. Parachute inflation parameter distributions are selected to sweep the range of values in literature for the specific parachute types and components used [9].

Capsule Design Decisions

This mission has three requirements: generate peak re-entry stagnation point heat fluxes in excess of 100 W/cm^2 , collect data during the heat pulse to aid in AMTPS material thermal response model improvement, and recover the capsule and forebody TPS intact. Analysis of flight mechanics simulation output data is used to drive mission architecture and capsule design to meet these objectives. The Mars Microprobe geometry [2], which is a 45-degree sphere-cone with a spherical cap backshell, is selected for the flight capsule OML for reasons discussed in subsequent sections of this paper. The flight capsule OML diameter cannot exceed 35.56 cm due to launch vehicle shroud constraints. Trade studies performed on capsule mass and forebody nose radius identify a nominal design that achieves a peak re-entry heat flux over

100 W/cm^2 . A 30 kg capsule provides a good balance between driving up ballistic coefficient to achieve higher peak heat fluxes and constraining aggregate capsule density to a level that can realistically be manufactured with the necessary on-board instrumentation, avionics, and parachute systems. A nose radius of 10% the capsule reference area diameter yields an estimated nominal peak cold-wall stagnation point heat flux of 135 W/cm^2 . This nose radius provides design margin over the mission requirement of 100 W/cm^2 peak heat flux while not deviating drastically from the heritage stability characteristics of the Mars Microprobe OML [2], which utilized a nose radius of 25% the capsule diameter. The subsection entitled "Capsule Aerodynamics Model" discusses flight stability impacts due to this deviation from the heritage design. Figure 6 depicts the OML geometry of the prototype flight capsule and identifies key measurements in the model drawing. Table 1 presents key capsule mass and geometric properties.

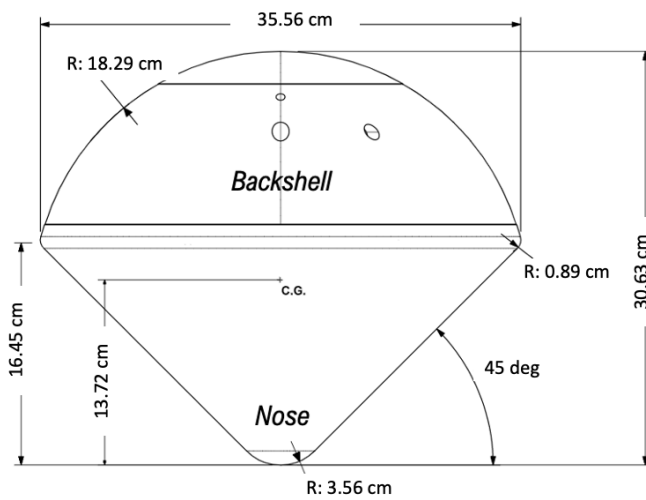


Figure 6: AMTPS prototype capsule dimensions.

Table 1: Prototype Capsule Properties

Parameter	Value
Forebody Cone Angle	45 deg
Capsule Diameter	35.56 cm
Mass	30.0 kg
Hypersonic Ballistic Coef.	300 kg/m^2
Nose Radius	0.1 Diam
Shoulder Radius	0.025 Diam
Backshell Radius	0.514 Diam
C.g. Axial Dist. from Nose	0.38 Diam

Ensuring the forebody TPS is oriented into the atmospheric flow when entry heating and pressure become appreciable is critical to mission success. The capsule is an unguided, ballistic entry vehicle with no means of actively controlling vehicle attitude. Additionally, the launch vehicle is not spin-stabilized on ascent, meaning the capsule will not be spin-stabilized after egress. To mitigate unfavorable attitudes during key atmospheric entry events, the capsule OML is designed in the same form factor as the heritage Mars Microprobe and the capsule center of gravity (c.g.) is judiciously placed. With a favorable c.g. location, the Mars Microprobe

OML possesses sufficient static and dynamic stability characteristics to self right from any exo-atmospheric orientation once appreciable atmosphere is encountered [2], [4]. The AMTPS capsule is ballasted with 20 kg of tungsten plates in the forward-most section of the capsule interior to achieve a center of gravity location 0.38 diameters from the vehicle nose and centered on the vehicle axis of symmetry. Figure 7 presents Monte Carlo simulation data for capsule total angle of attack at peak entry heat flux. The exo-atmospheric capsule orientation at egress from the launch vehicle is dispersed within the simulation using data provided by the launch provider; total angle of attack at egress ranges between 142 degrees and 180 degrees. The capsule recovers from dispersed exo-atmospheric orientations to trim at angles of attack less than 2.9 degrees in 99% of cases by the point of peak heating.

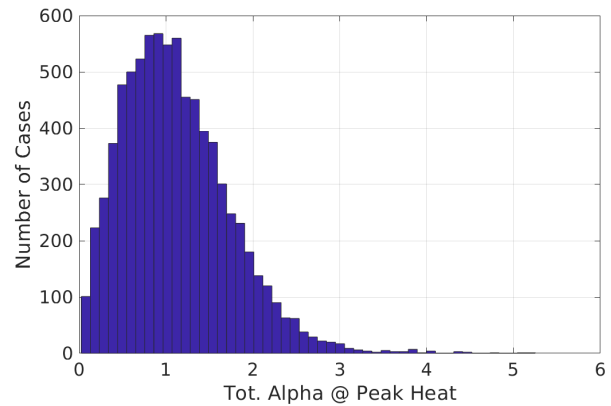


Figure 7: Histogram of capsule total angle of attack at peak heat flux conditions from an 8001 case Monte Carlo analysis.

Capsule Aerodynamics Model

Aerodynamic modeling of the AMTPS capsule is accomplished using the database of aerodynamic coefficients developed for Mars Microprobe flight mechanics simulations [3]. Modifications to that database are incorporated to reflect the differences in AMTPS capsule and mission. Specifically, the modified Newtonian aerodynamic coefficients used to model tumbling and hypersonic flight aerodynamics are adjusted for an Earth atmosphere by simply replacing the normal-shock stagnation pressure coefficient with its corresponding value for air. To capture effects of the reduced spherical nose radius on supersonic aerodynamics, the tabulated wind tunnel data [12] used in the Mars Microprobe aerodynamics database [2] were revisited. These tests collected data at various nose radii, enabling the existing aerodynamic coefficients to be replaced with data corresponding to a nose radius equal to 12.5% capsule diameter. This was considered sufficiently close to the AMTPS nose radius of 10% capsule diameter to capture any effects on capsule aerodynamics. Ultimately – for the 45 degree sphere-cone – these wind tunnel data indicated that reductions in nose radius below the 25% capsule diameter size had very little effect on the aerodynamic coefficients.

While the changes in OML relative to Mars Microprobe are expected to have a negligible effect on capsule stability, the AMTPS center of gravity is located farther aft. Relative to the Mars Microprobe design, this has a destabilizing effect in the nose-forward orientation and is stabilizing in the aft-forward orientation. Performing a complete re-assessment of AMTPS capsule static and dynamic stability is beyond

the scope of this project; however, several relevant and successful test flights have been conducted as part of the Reentry Breakup Recorder (REBR) capsule design developed by The Aerospace Corporation [4]. The REBR OML was also based on the Mars Microprobe and additional subsonic wind tunnel testing was performed to establish static stability limits related to axial center of gravity location. The REBR c.g. was located approximately 0.4 capsule diameters aft of the nose, which is further aft than the AMTPS value of 0.38 capsule diameters. During its flight test onboard the Japanese HTV2 supply vehicle, the REBR capsule was shown to have recovered from tumbling orientation during reentry, and remained in stable flight until ocean impact. While the REBR flight tests do not aide in aerodynamic modeling for AMTPS, they do provide a measure of confidence that stability characteristics of the AMTPS prototype flight test capsule. Further iteration on the AMTPS OML could work to redesign the spherical aftbody with a curvature center located at the capsule c.g. As established for the Mars Microprobe capsule design, this would help ensure self-righting capability and improved dynamic stability.

On-Board Capsule Instrumentation

The test flight primary goals are to assess the TPS performance and collect data to improve the thermal response model of the AMTPS material. On-board instrumentation is imperative to achieving both of these goals; this section discusses the various on-board instruments, their individual measurement ratings, and presents flight mechanics analysis to justify their selection and suitability to meet mission goals. Meaningful and useful post-flight inspection of the charred TPS material may only be achieved by coupling the inspection results with flight data identifying the duration and type of heating environment experienced. Thermal response model improvement similarly needs estimates of the encountered heating environment combined with in-depth TPS temperatures and recession data. The capsule contains the following on-board instrumentation to meet the flight test goals:

- 12 in-depth forebody thermocouples
- 5 external forebody pressure sensors [13], [14]
- 1 3-axis +/- 100 g accelerometer [15]
- 1 9-axis +/- 16 g accelerometer, +/- 2000 deg/s gyroscope, +/- 200 μ T magnetometer [16]
- 1 Javad TR-G2 GPS [17]
- 1 internal pressure sensor
- 1 internal temperature sensor
- 1 internal humidity sensor
- 1 Iridium satellite modem [18]

Figure 8 depicts an engineering model image of the capsule forebody structure (TPS layers not depicted) and identifies thermocouple (TC1-3) and pressure sensor (P1-5) locations. The capsule is designed as a ballistic re-entry vehicle that nominally trims at 0 deg angle of attack. The atmospheric flow impinging on the capsule forebody will produce a flow stagnation point near the vehicle nose (geometric center of the forebody as viewed in the figure). The stagnation point is instrumented with 1 pressure sensor (P1) and one thermocouple group (TC1) consisting of 3 co-located thermocouple wires at varying TPS depths. Pressure sensors P3 and P5 are placed midway between the forebody nose and shoulder while pressure sensors P2 and P4 are placed just inward of the forebody shoulder. Pressure sensor locations are selected to enable angle of attack reconstruction from pressure data. Thermocouple group 2 (TC2) is placed inward from the midway P3 pressure sensor. Thermocouple group 3 (TC3)

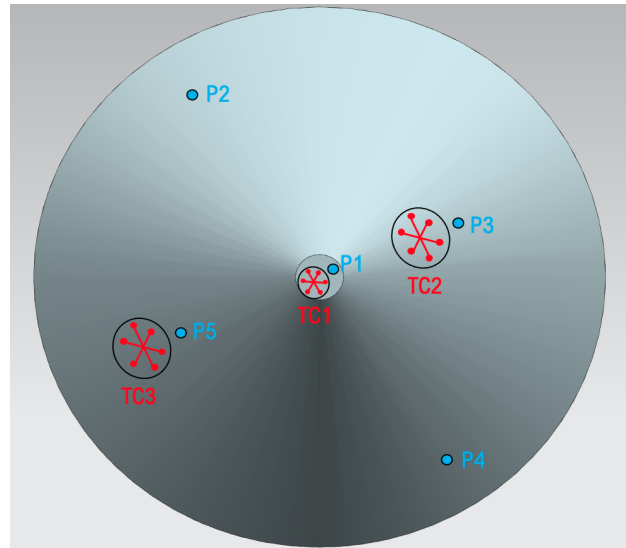


Figure 8: Diagram of capsule forebody thermocouple (TC1-3) and pressure sensor (P1-5) layout. Each thermocouple group consist of 3 thermocouples (represented by straight lines terminating in dots) at varying depths in the TPS. The capsule diameter is 35.56 cm.

is placed outward from pressure sensor P5. These locations provide a diverse view of temperature variations across the forebody and through the TPS layers during flight. This data will be use in post-flight trajectory and thermomechanical analysis to improve the AMTPS material thermal response model.

Figure 9 presents a Monte Carlo analysis distribution of peak stagnation point heat fluxes. The 1.0 percentile value of this distribution is 129 W/cm^2 . The predicted value of peak stagnation point heat flux is highly sensitive to underlying aerothermodynamic modeling assumptions used to generate the prediction. The mission and capsule are designed with an approximately 30% margin over the project heat flux requirement to protect against over-prediction of the cold-wall heat flux by the modeling assumptions used in this analysis, namely the cold-wall boundary condition assumptions inherent in Sutton-Graves equations. At these cold wall heat fluxes, material response thermal analysis predicts a peak stagnation point surface temperature of approximately 1800K and peak surface temperatures at the vehicle flank of 1400K. This analysis is used to inform thermocouple type selection. Two types of thermocouples are considered, TypeR and TypeK; TypeR thermocouples possess higher temperature ratings but have a lower signal to noise voltage ratio as compared to TypeK. Thermal analysis predicts peak temperatures over the entire forebody will fall within the qualification range for TypeK thermocouples. Therefore, TypeK thermocouples are selected for all TC locations shown in Figure 8, except for the outer-most depth at the stagnation point, for which a TypeR TC is selected to provide extra margin at the predicted hottest part of the capsule during entry. Section 5 presents a more rigorous approach to aerothermal analysis that indicates the Sutton-Graves equations overpredict the peak heat flux condition by 21%. However, even after extrapolating this error correction to the Monte Carlo Sutton-Graves heat flux estimates, the project requirement of 100 W/cm^2 is still achieved in 99% of all cases.

Figure 10 displays a Monte Carlo analysis distribution of

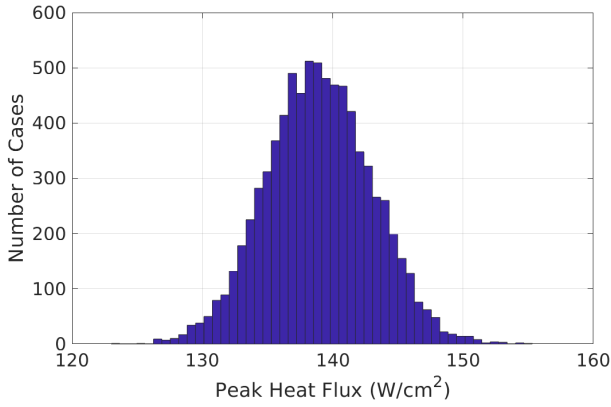


Figure 9: Histogram of peak stagnation point heat flux (Sutton-Graves) from an 8001 case Monte Carlo analysis.

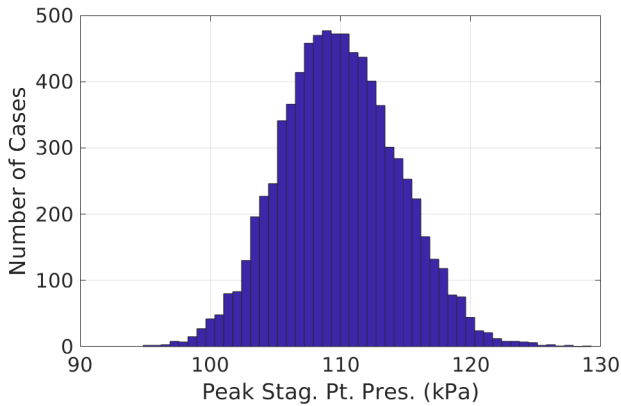


Figure 10: Histogram of peak stagnation point pressure from an 8001 case Monte Carlo analysis.

peak stagnation point pressures. Stagnation point pressures are calculated using chemical equilibrium analysis [8]. Peak pressures less than 130 kPa are anticipated for all flight conditions. Based on this analysis, absolute pressure sensors rated for 0 - 160 kPa are selected to instrument near the nose of the forebody and pressure sensors rate for 0 - 103 kPa are selected to instrument the forebody away from the nose.

Figure 11 shows the sensed acceleration for the nominal entry trajectory. Three spikes in sensed acceleration are present. The largest spike corresponds to the capsule deceleration in the upper atmosphere at high dynamic pressures. The subsequent two spikes correspond to the drogue and main parachute deployments. The capsule is equipped with two inertial measurement units (IMU's): one 16g (low-g) and one 100g (high-g) IMU. Both IMU's are synchronized in time; the low-g unit will capture 93% of the entry flight time with finer acceleration resolution while the high-g unit will capture short spikes in acceleration during launch (not shown in Figure 11), peak entry deceleration, and parachute deployments. Monte Carlo analysis shows the 99th percentile peak sensed descent acceleration to be 23.8 g 's, see Figure 12. Mean, 1.0 percentile, and 99.0 percentile statistics for peak heat flux, peak stagnation point pressure, and peak sensed acceleration are collected in Table 2.

In addition to the instrumentation discussed above, the cap-

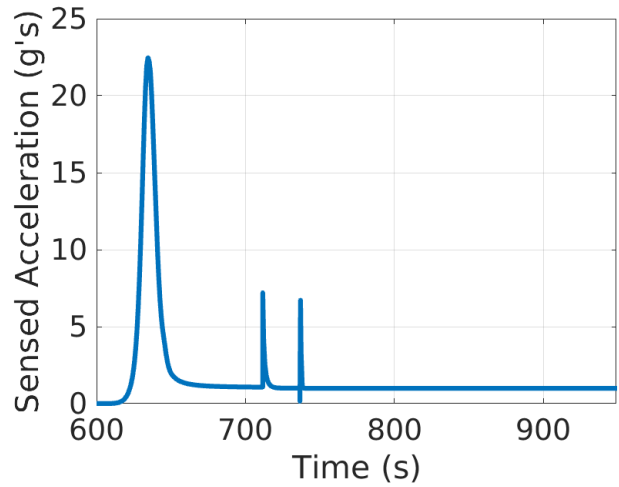


Figure 11: Sensed acceleration (in Earth g 's) for the nominal capsule entry trajectory. As time increases, the three acceleration spikes correspond to peak atmospheric deceleration, drogue parachute deployment, and main parachute deployment, respectively.

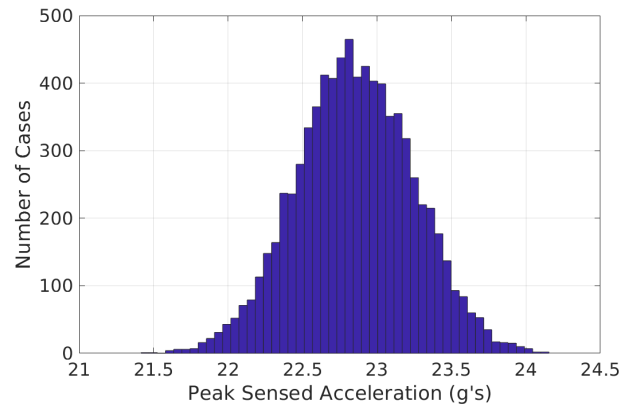


Figure 12: Histogram of peak sensed acceleration (in Earth g 's) from an 8001 case Monte Carlo analysis.

sule is equipped with internal temperature, pressure, and humidity sensors, a GPS unit, and an Iridium satellite modem. The internal temperature, pressure, and humidity sensors are used to reconstruct the operating environment of the capsule electronics and internal subsystems. The internal pressure sensor is also used to trigger drogue parachute deployment based on altitude. The on-board GPS is a military-grade, Javad TR-G2 unit that is not operationally limited by altitude, as many commercially-available civilian units are. It has a 21 gram mass and 100 Hz update frequency. The GPS data will be blended with IMU data to enhance post-flight reconstruction of the capsule trajectory. An on-board satellite modem will connect to the Iridium satellite network during the parachute descent phase of flight to relay GPS coordinates to ground operations staff who will use the data to aid capsule recovery operations after touchdown.

Two-Stage Parachute System Simulation and Design

To preserve the structural integrity of the charred heatshield and on-board instrumentation data storage at ground impact, a two-stage parachute descent system is designed to achieve

Table 2: Entry Event Peak Value Statistics

Parameter	1%-tile	Mean	99%-tile
Heat Flux (W/cm^2)	129	139	148
Stag. Pt. Pres. (kPa)	100	110	121
Sensed Accel. ($g's$)	21.9	22.9	23.8

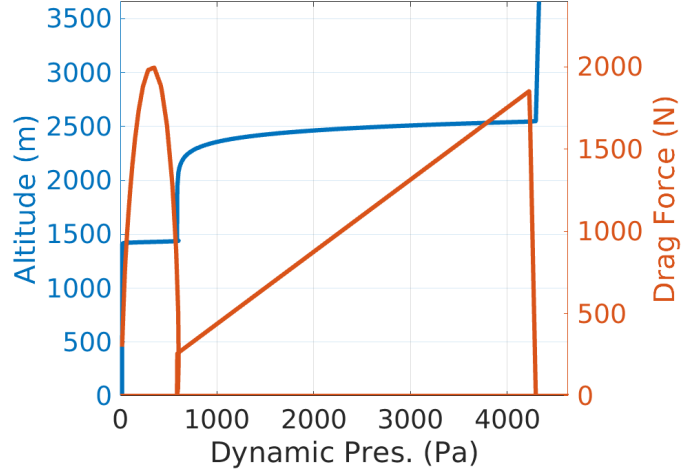
benign capsule velocity at surface touchdown. Structural analysis of the capsule during ground impact showed the TPS is conservatively resistant against failure at total velocities of 15 m/s for contact attitudes between 0.0 and 5.0 degrees off-orthogonal. The analysis used experimentally-determined material properties for the outer, inner, and adhesive layers of the TPS, both virgin and charred. To ensure the integrity of the on-board instrumentation data, a shock resistant solid-state memory card was selected to house the data captured throughout flight. Analysis indicates this storage device will survive impact velocities under 15 m/s. To further increase the factor of safety on the memory card, the capsule interior will be filled with syntactic foam to provide extra support to internal avionics components. A planned vibration test campaign will further qualify the avionics design's tolerance of expected vibration loads during the flight test.

Parachute deployment is modeled using a fixed inflation distance assumption [9]. Equation 1 gives the relationship between instantaneous parachute diameter (D_{inst}), capsule velocity (V), and parachute inflation factor (p_{inf}) during the inflation phase of flight. The time required to reach full inflation (t_f) is given in Equation 2, where D_{max} is the fully inflated parachute diameter.

$$D_{inst} = \frac{V}{p_{inf}} \quad (1)$$

$$t_f = \frac{D_{max} p_{inf}}{V} \quad (2)$$

The above relations are used to model the time-dependent inflation loads of both the drogue and main parachutes. Figure 13 shows parachute drag force and altitude versus dynamic pressure for the simulated nominal trajectory. The drogue parachute is deployed at 2550 m altitude above the geoid, detected using an internal barometric pressure sensor. Peak drogue force of 1851 N occurs at Mach 0.34 and 4228 Pa dynamic pressure. Peak main parachute force of 1994 N occurs 25 s later at Mach 0.12 and 350 Pa dynamic pressure. Parachute diameters, deployment Mach numbers, and deployment dynamic pressures are tuned to achieve desired limits on touchdown velocity while maximizing the minimum parachute system safety factor during operation. Specifications and pertinent characteristics of both parachutes are presented in Table 3. Table 4 contains statistics on peak opening loads for the drogue and main parachutes from a Monte Carlo analysis of 8001 runs. The 99th-percentile loads are 2006 N and 2493 N, respectively. These 99th-percentile flight loads result in system minimum safety factors of 2.5 and 3.2 for the drogue and main parachute, respectively, when compared against manufacture rated and experimentally determined strengths of parachute suspension lines, riser lines, shock cords, bridle lines, and all linkages and connection points between the various parachute components as well as between the bridle lines and their anchor points to the capsule.

**Figure 13: Nominal parachute drag force and altitude above geoid versus dynamic pressure.****Table 3: Parachute System Characteristics**

Parameter	Drogue Chute	Main Chute
Parachute Type	Elliptical	Annular
Diameter (cm)	61	305
Drag Coefficient	1.5	2.2
Num. Suspension Lines	8	12
Num. Shock Cords	1	0
Num. Harness Lines	3	4
Num. Linkages	4	3

Figure 14 displays the touchdown velocity distribution from a Monte Carlo trajectory analysis. The mean and 99th percentile touchdown velocities are 7.9 m/s and 12.1 m/s, respectively. The peak impact speed falls under the project requirement of 15 m/s necessary to preserve the structural integrity of the charred TPS during impact.

5. AEROTHERMODYNAMIC ANALYSIS

The Sutton-Graves predictions, presented in Section 4, provide an acceptable approximation of the peak heat flux, however, a higher fidelity approximation of the peak heat flux is found through the use of hypersonic computational fluid dynamics (CFD). One common CFD tool used for this purpose is the Data Parallel Line Relaxation (DPLR) Code [19]. DPLR is a structured, finite volume, non-equilibrium Navier–Stokes flow solver. The code contains the ability to modify the grid domain to ensure the grid is aligned with the shock wave.

In order to simulate the peak heat flux, characteristics of the

Table 4: Peak Parachute Force Monte Carlo Statistics

Parameter	1%-tile	Mean	99%-tile
Peak Drogue Force (N)	1691	1839	2006
Peak Main Chute Force (N)	1590	1952	2493

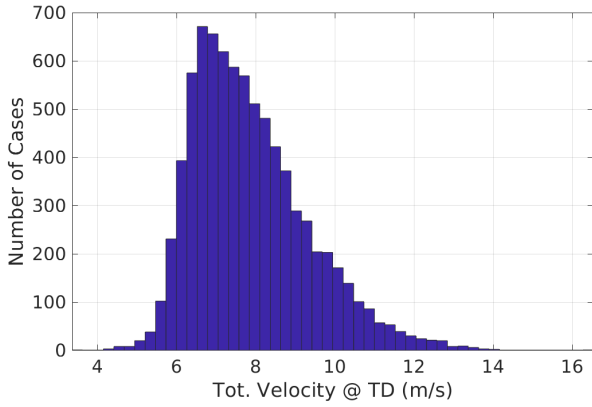


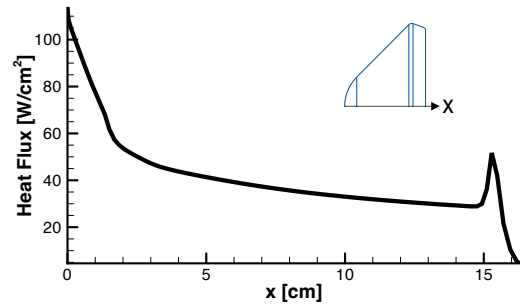
Figure 14: Histogram of total velocity at touchdown.

flow must be known at peak heat flux time. This information is gathered from the trajectory in Section 4. The time of peak heat flux was found at 570.7 s within the nominal trajectory where the entry capsule is moving at a velocity of 2.256 km/s. The ambient conditions at this altitude are as follows: density = 1.16×10^{-2} kg/m³ and temperature = 231 K. Since the vehicle is traveling through the Earth’s atmosphere, a five species air model (N, N₂, O, O₂, NO) was utilized. These parameters are used to initialize the free stream within DPLR.

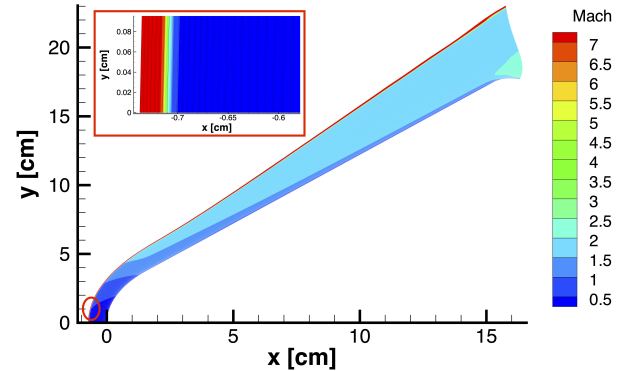
At the windward surface of the capsule, the boundary conditions are more subjective. For this study, a cold wall boundary condition is assumed since it more closely relates to the assumptions made in the Sutton-Graves formulation. In addition to a cold wall boundary condition, the wall is assumed to be fully catalytic. DPLR is run until the solution completely converges and the grid adequately adapts to the bow shock. The results of these simulations are presented in Figures 15a and 15b.

Figure 15a shows the projected DPLR heat flux, in W/cm² over the profile of the vehicle. The highest heat flux for this vehicle is recorded at the stagnation point, which for this vehicle is located at $x = 0$ cm. Passing the stagnation point, the heat flux experiences a steep decrease in heat flux reaching approximately 40 W/cm² at the crease of the heat shield. It is not until the shoulder of the vehicle, $x \sim 15$ cm, that the heat flux peaks back up to 55 W/cm² then dissipating to lower values as the flow passes to the backshell of the vehicle.

Figure 15b presents the mach number over the profile of the vehicle. In this figure the local peak mach number at this flow condition, $M=7$, is represented in the red, while dark blue indicates where the mach number is zero and thus stagnant. As expected, the flow is completely stagnant at $x = 0$ cm and increases as the x and y axis increase along the profile. At the shoulder of the vehicle, it is now clear to see why there is localized heating in Figure 15a in this same region. The flow begins to expand, increasing gas velocity and driving higher heating in this region. Figure 15b also provides an enhanced view of the flow to show the free stream, shock layer, boundary layer transition. As to be expected, the free stream mach number abruptly decreases to boundary layer, thus creating a bow shock layer. This trend can be found through examining the entire bow shock and is one indicator to the DPLR user that the problem has fully converged.



(a) Heat flux [W/cm²] along the profile of the vehicle forebody (x [cm]).



(b) Mach number over the profile of the vehicle forebody (x [cm], y [cm]) showing the bow shock location.

Figure 15: CFD localized mach and heat flux data for capsule at peak heat flux flight condition.

Finally, the peak heat flux for this geometry is found to be 109.79 W/cm², which is 21% less than the Sutton-Graves formulation prediction of 139 W/cm², as shown in Section 4. While the predictive differences between the methods are appreciable, both methods show that the geometry meets the mission objectives of testing the AMTPS material at peak heat fluxes over 100 W/cm².

6. PROTOTYPE CAPSULE FABRICATION STATUS

Prototype capsule fabrication and assembly is nearing completion; however, several key milestones need first be reached. The capsule forebody structure has been 3D printed out of alluminum, machined to the desired finish, and had holes tapped for TC and pressure sensors infusion. Tungsten plates have been procured, machined, and mounted in the forward section of the forebody as ballast. All instrumentation sensors and components have been procured; all but the TC and pressure sensors have been integrated in to the capsule. Avionics logic boards and software have been designed, manufactured, and successfully completed all functionality tests except the TC and pressure transducers functionality tests. These tests must be performed after the TPS is printed on to the forebody structure. The parachute system, consisting of the parachute canopies, lines and linkages, compressed gas deployment system, and release mechanisms, have been designed, procured, experimentally tested, and functionally certified for flight. The backshell has been 3D printed out of Ultem and integrated with the capsule forebody, interior avionics, and interior parachute subsystem. The integrated capsule has undergone functionality tests to make sure the

avionics can get good readings from the instrumentation and the parachute system can successfully complete the deployment sequence.

7. FURTHER WORK

Capsule testing and integration work is currently paused until the TPS is printed and cured onto the capsule forebody structure. The TPS additive manufacturing process has undergone several revisions as engineers tune the material formulation to achieve desired material properties. The adhesive layer between the capsule structure and the insulative TPS layer has proven particularly challenging to achieve good adhesion after the curing process. The TPS team is currently on track to complete the prototype capsule TPS print by February 2023. Following the completion of the forebody TPS print, capsule integration activities will resume with the installation of TC and pressure sensors into the forebody TPS followed by completion of instrumentation and avionics integration and functionality tests. After all avionics and instrumentations test have been completed, the internal capsule volume around the avionics will be filled with syntactic foam to increase hardware structural resilience to flight loads, vibrations, and ground impact. A vibration testing campaign will be the final test completed on the prototype capsule. Lessons learned will be incorporated into any design modifications for a planned flight hardware capsule build.

At the outset of the AMTPS project, the launch vehicle procurement and flight operations were fully funded. However, funding cuts at NASA's Science Mission Directorate have filtered down to this project resulting in significantly reduced funding. The project is currently exploring partnership opportunities to make up the difference in funding before progressing beyond the prototype capsule to the flight hardware capsule build.

The details of the capsule mechanical design, structural analysis, fabrication, experimental testing campaigns, and flight certification will be the subject of a subsequent paper.

8. SUMMARY

A flight mechanics overview is presented of an Earth flight test mission designed to test a novel, 3D printed thermal protection system that is currently in development at NASA as part of a multi-center Early Career Initiative effort for the Additive Manufacturing of Thermal Protection Systems project. The flight test objectives are to subject the forebody stagnation point of a capsule equipped with additively manufactured TPS material to peak heat fluxes in excess of 100 W/cm^2 , capture in-flight data to enable flight reconstruction and AMTPS material thermal response model improvement, and recover the capsule with data storage and forebody AMTPS intact to enable post-flight inspection and analysis of AMTPS performance.

The capsule and flight trajectory are designed such that the proposed flight test exceeds the project requirement heat flux by 29% in 99% of cases based on cold-wall boundary condition assumptions of Sutton-Graves estimates and Monte Carlo analysis using current best-estimate flight simulation dispersions. CFD analysis indicates that Sutton-Graves approximations may overestimate heat fluxes by 21% at the peak heat flux condition of the nominal flight trajectory. Extrapolating this error to off-nominal trajectories, the flight

test still exceeds the project requirement in 99% of cases due to design margin built into the mission from conception.

The capsule is equipped with sufficient instrumentation to capture forebody pressures and in-depth temperatures across the capsule forebody during the entry heat pulse. The avionics system is capable of recording this heat pulse data along with IMU and GPS data to enable reconstruction of the flight trajectory and aerothermal environment over the entire duration of the flight test. This data will provide useful insight into the AMTPS material behavior during an entry environment relevant to a wide variety of entry, descent, and landing applications.

A two-stage recovery system is designed with sufficient factors of safety to decelerate the capsule to ground impact velocities shown to be non-destructive to virgin and charred AMTPS material as well as to the onboard data storage repository.

This paper demonstrates that an entry trajectory and entry capsule equipped with the novel AMTPS material have been designed to meet all flight test project requirements in 99% of off-nominal, dispersed flight conditions. Based on the flight mechanics analysis presented in this paper, a prototype capsule has been fully designed and is nearing manufacturing and integration completion.

ACKNOWLEDGMENTS

The authors offer sincerest thanks to the following individuals for their contributions to this body of work. Mykale-Jamal Holland of NASA Johnson Space Flight Center (JSC) is a core project member responsible for the capsule structural design. University of Kentucky Ph.D. graduate student, Matthew Ruffner, is a core project member responsible for the design and build of the avionics systems and functionality test campaign. University of Kentucky graduate student, John Schmidt, is a core project member responsible for the design and build of the parachute system and handled the bulk of capsule hardware procurement, integration, and testing. Richard Hagen of NASA JSC mentored and assisted in the hardware design, build, and testing. Sydney Taylor of NASA JSC is a core team member responsible for exo-atmospheric passive thermal analysis of the capsule. Som Dutta of NASA Langley Research Center (LaRC) provided mentorship on the flight mechanics modeling and systems engineering. Jared Daum of NASA JSC offered his time and expertise to inform and review the parachute design and experimental test campaigns. Rohan Deshmukh of NASA LaRC provided assistance with instrumentation selection.

REFERENCES

- [1] A. T. Sidor, E. Venkatapathy, and S. A. Bouslog, "NASA Efforts to Explore Additively Manufactured Thermal Protection Systems (AMTPS)," 2nd International Conference on Flight Vehicles, Aerothermodynamics and Re-entry Missions Engineering (FAR), 2022.
- [2] R. A. Mitcheltree, R. D. Braun, F. M. Cheatwood, F. A. Greene, and J. N. Moss, "Aerodynamics of the Mars Microprobe Entry Vehicles," *Journal of Spacecraft and Rockets*, vol. 36, pp. 392–398, 1999, doi: 10.2514/2.3458.
- [3] R. D. Braun, R. A. Mitcheltree, F. M. Cheatwood,

“Mars Microprobe Entry-to-Impact Analysis,” Journal of Spacecraft and Rockets, vol. 36, pp. 412–420, 1999, doi: 10.2514/2.3461.

- [4] M. A. Weaver, W. H. Ailor, ”Reentry Breakup Recorder: Concept, Testing, Moving Forward, AIAA SPACE 2012 Conference & Exposition, AIAA 2012-5271, Sep. 2012, doi: 10.2514/6.2012-5271.
- [5] R. A. Lugo, J. D. Shidner, R. W. Powell, S. M. Marsh, J. A. Hoffman, D. K. Litton, and T. L. Schmitt, ”Launh Vehicle Ascent Trajectory Simulation Using the Program to Optimize Simulated Trajectories II (POST2),” AAS/AIAA Space Flight Mechanics Meeting, February 2017.
- [6] NASA Earth Fact Sheet: <https://nssdc.gsfc.nasa.gov/planetary/factsheet/earthfact.html>
- [7] Earth Global Reference Atmospheric Model 2010: <https://software.nasa.gov/software/MFS-32780-1>
- [8] S. Gordon and B. J. McBride, ”Computer Program for Calculation of Complex Chemical Equilibrium Compositions and Applications,” NASA Reference Publication 1311, 1996.
- [9] T. W. Knacke, ”Parachute Recovery Systems Design Manual,” Naval Weapons Center China Lake CA, 1991.
- [10] A. Cassell, P. Wercinski, B. Smith, B. Yount, O. Nishioka, and C. Kruger, ”ADEPT Sounding Rocket One Flight Test Overview,” Jun. 2019, pp. 1–15. doi: 10.2514/6.2019-2896.
- [11] S. Dutta et al., ”Adaptable Deployable Entry and Placement Technology Sounding Rocket One Modeling and Reconstruction,” J Spacecraft Rockets, vol. 59, no. 1, pp. 1–24, 2021, doi: 10.2514/1.a35090.
- [12] J. O. Nichols and E. A. Nierengarten, ”Aerodynamics Characteristics of Blunted Bodies,” Jet Propulsion Lab., TR 32-677, California Inst. of Technology, Pasadena, CA, Feb. 1964.
- [13] Honeywell 103 kPA Pressure Sensor: <https://www.digikey.com/en/products/detail/honeywell-sensing-and-productivity-solutions/sscsrnn1-6ba7a3/2416214>
- [14] Honeywell 160 kPA Pressure Sensor: <https://www.digikey.com/en/products/detail/honeywell-sensing-and-productivity-solutions/sscsrnn1-6BA7A3/2416214>
- [15] ST Microelectronics H3LIS100DL high-g IMU: <https://www.st.com/en/mems-and-sensors/h3lis100dl.html>
- [16] InvenSense ICM-20948 low-g IMU: <https://invensense.tdk.com/products/motion-tracking/9-axis/icm-20948/>
- [17] Javad TR-G2 GPS unit: <https://www.javad.com/jgnss/products/oem/TR-G2/specifications.html>
- [18] NAL Research Iridium Modem: <https://www.nalresearch.com/product/a3la-rs/>
- [19] M. J. Wright, G. V. Candler, and D. Bose, ”Data-Parallel Line Relaxation Method for the Navier–Stokes Equations,” AIAA Journal, Vol. 36, No. 9, Sept. 1998, pp. 1603–1609. doi:10.2514/2.586

BIOGRAPHY



David J. Blette received his Ph.D and M.S. degrees in Aerospace Engineering from Georgia Tech and his B.S. degree in Aerospace Engineering and Mechanics at the University of Minnesota – Twin Cities. He is currently a Flight Mechanics Engineer at the Atmospheric Flight and Entry Systems Branch at NASA Langley Research Center and serves as the Flight Test Lead for the Additive Manufacturing of Thermal Protection Systems project. His interest include flight mechanics and systems engineering for atmospheric entry, descent, and landing.



Adam Sidor has a M.S. and Ph.D. degrees in Aerospace Engineering from Georgia Tech and a B.S. in Mechanical Engineering from Cornell University. He is an engineer in the Thermal Design Branch at NASA Johnson Space Center. Adam has lead the Additive Manufacturing of Thermal Protection Systems project as the principal investigator. His work and interests center on design and manufacturing of thermal protection systems (TPS), particularly streamlining build and integration of TPS.



John E. Theisinger has received his M.S. degree in Aerospace Engineering from Georgia Tech and his B.S. degree in Aerospace Engineering from Texas A&M University. He is currently an Aerodynamicist in the Atmospheric Flight and Entry Systems Branch at NASA Langley Research Center and serves as the Aerodynamics Lead for the Additive Manufacturing of Thermal Protection Systems project. His work focuses on aerodynamics analyses and development of force and moment databases for atmospheric entry, descent, and landing applications.



Ali D. Omidy received his B.Sc. and Ph.D degree in Mechanical Engineering from the University of Kentucky. He is currently a Thermal Engineer at the Thermal Design Branch at NASA Johnson Space Center. Ali serves as the Aerothermal Lead for the Additive Manufacturing of Thermal Protection Systems project. His interest include thermal designs for atmospheric entry, descent, and landing purposes.